The Meteoritical Society

Meteoritics & Planetary Science 47, Nr 11, 1789–1808 (2012)
doi: 10.1111/maps.12013

IRTF observations of S complex and other asteroids: Implications for surface compositions, the presence of clinopyroxenes, and their relationship to meteorites

Katherine M. GIETZEN[1], Claud H. S. LACY[1,2], Daniel R. OSTROWSKI[1], and Derek W. G. SEARS[1,3,4*]

[1]Arkansas Center for Space and Planetary Sciences, University of Arkansas, Fayetteville, Arkansas 72701
[2]Department of Physics, University of Arkansas, Fayetteville, Arkansas 72701
[3]Department of Chemistry and Biochemistry, University of Arkansas, Fayetteville, Arkansas 72701
[4]Present address: Space Science and Astrobiology Division, MS245-3, NASA Ames Research Center, Moffett Field, Mountain View, California 94035, USA
*Corresponding author. E-mail: derek.sears@nasa.gov

(Received 22 February 2011; revision accepted 26 September 2012)

Abstract–We have obtained near-infrared spectra for near-Earth asteroids (NEA) and Main Belt asteroids by using NASA's Infrared Telescope Facility. Most of the S complex classes of the Tholen-Bus-DeMeo scheme and the S(I)–S(VII) classes are represented. To help interpret the results, we examined visible/near-IR spectra for ordinary chondrites. The unequilibrated ordinary chondrites (UOC) spectra contain a 2.3 μm feature which is absent in the spectra of the equilibrated ordinary chondrites (EOC). On the basis of literature data and new spectra low-Ca clinopyroxenes, we suggest that the 2.3 μm in UOC is due to the presence of low-Ca clinopyroxene in the UOC which is absent in EOC. While this difference can be seen in the raw spectra, we confirmed this observation using a modified Gaussian model (MGM) for spectral analysis. Both the UOC and the EOC plot in the S(IV) field of the band area ratio plot for asteroids. We suggest that many or most S(IV) asteroids have material resembling UOC on their surfaces. An internally heated ordinary chondrite parent object would have EOC material at depth and UOC material on the surface. Cosmic ray exposure ages, and K-Ar ages for L chondrites, indicate that most EOC came from relatively few objects; however, the age distributions for UOC are unlike those of EOC. We suggest that while EOC come from the interiors of a limited number of S(IV) asteroids, the UOC come from the surfaces of a large number of S(IV) asteroids.

INTRODUCTION

Asteroids are clearly the remnants of materials from which the planets formed (Bottke et al. 2002). Yet they are highly diverse, reflecting a variety of nebular and early solar system processes (Bus et al. 2002; Gaffey et al. 2002; Hilton 2002). Considerable insights into their history and present nature have been provided by recent missions (Belton et al. 1992, 1994; Sullivan et al. 1996; Thomas et al. 1999, 2002; Robinson et al. 2002), especially near-Earth asteroids (NEAs) with their relative ease of access (Farquhar et al. 2002) and interest as potentially hazardous objects (Belton et al. 2004). Knowledge of their composition is critical in understanding their scientific implications for solar system history, and for impact mitigation efforts. In the absence of returned samples, the primary sources for compositional data for asteroids are reflectance spectra obtained by spacecraft and, mostly, ground-based observations. Spectra in the visible wavelength range (0.4–0.9 μm) have been available for some time and elaborate classification systems based on these are available (e.g., Tholen 1989; Bus and Binzel 2002). However, in recent years data in the visible range has been supplemented with spectra in the near-infrared wavelengths (0.8–2.5 μm), most notably by astronomers utilizing the NASA Infrared Telescope Facility. The inclusion of this wavelength range not only allows improved taxonomy (DeMeo et al. 2009) but also provides mineralogical information (Gaffey et al. 1993).

Unfortunately, while there are over 5000 known NEAs, near-IR spectra are available for only about 1.5%.

To describe and help understand this diversity, considerable effort has been put into taxonomy. Existing classification schemes divide the asteroids into three complexes, which are further divided into individual classes. (1) The C complex (B, C, Cb, Cg, Cgh, Ch) with low albedos and essentially featureless spectra, which comprise approximately 25% of the total asteroid population. (2) The X complex (X, Xc, Xe, Xk) with nearly featureless and linear spectra, but steeper near-IR continua than C asteroids, which make up approximately 19% of the total asteroid population. (3) The S complex asteroids (A, D, K, L, Ld, R, S, Sa, Sk, Sl, Sr, T, V) with their high albedos and deep absorption bands constitute about 56% of the total asteroid population with approximately 35% of the total asteroid population being S asteroids (S, Sa, Sk, Sl, Sr). A long-standing challenge has been to explore the extent to which the great many meteorite classes can be associated with the great many asteroid classes (see Burbine et al. 2002, and the references therein).

To a first order approximation, the near-IR spectra of S asteroids are dominated by two bands, a broad band at about 1 μm caused by pyroxene and olivine absorptions, and a broad band at about 2 μm caused predominantly by pyroxene. Of course, variations in the compositions of these minerals and the presence of minor minerals such as metal and plagioclase can affect the position and width of these two bands. Previous workers have quantified the effect of Fe, Mg, and Ca on peak positions[1] (Klima et al. 2007, 2011), noting particularly the different spectral properties of high-calcium pyroxene (HCP) relative to low-calcium pyroxene (LCP); the bands are at about 0.92 and about 1.85 μm for LCP and at about 1.03 and 2.30 μm for HCP.

There is a potential for confusion in using the terms HCP and LCP. We show below that UOC contain low-calcium pyroxene in the monoclinic form with spectra resembling those of HCP that are invariably monoclinic. Apparently, it is the structure of the pyroxene rather than its Ca content that is determining the position of the peaks, although exact peak positions are influenced by cation content. We will therefore refer to clinopyroxenes (CPX) and orthopyroxenes (OPX) in the present paper and avoid the terms HCP and LCP.

In an effort to go beyond descriptive taxonomy and address mineralogical questions, Gaffey et al. (1993a) divided the S asteroids into types S(I) through S(VII). Their approach is to produce a plot of the position of approximately 1 μm band against the ratio of the area of approximately 1 and 2 μm bands. Following the Gaffey et al. (1993a) work, we will refer to this diagram as the band area ratio (BAR) plot. The mineralogical interpretations of this plot were discussed at some length by Gaffey et al. (1993b). When plotted on the BAR plot, meteorites plot in the fields in essential agreement with their known mineralogy, thus basaltic achondrites plot just above the S(VII) field on the right side (the pyroxene side) of the diagram and the ordinary chondrites plot in the S(IV) field, these meteorites being a more-or-less equal mix of pyroxenes and olivines. For many of the asteroid classes there are no meteorite counterparts and Gaffey and coworkers have argued that these represent melts or partial melts not sampled by Earth (Gaffey et al. 1993, 2002; Sunshine et al. 2004; Gaffey 2007). This proposal is based on the fact that the spectra contain clinopyroxene bands normally associated with high-Ca pyroxenes, which, in turn, are associated with igneous rocks, meteoritic, and terrestrial.

Mineralogical interpretation of the near-IR spectra is also possible by reducing the spectral bands to individual Gaussian curves using, for example, the modified Gaussian model (MGM) of Sunshine and Pieters (1993). This method enables a more quantitative description of the reflectance spectra and, with laboratory data for comparison materials like terrestrial minerals and meteorites, can help identify and characterize the minerals responsible for the spectra.

Of particular interest to us is the relationship between ordinary chondrites, in particular the unequilibrated ordinary chondrites, and the S asteroids. The distinction between equilibrated and unequilibrated ordinary chondrites lies in the heterogeneity of mineral composition, distinctness of structural features, like chondrules, and recrystallization and coarsening of initially fine-grained materials. These features indicate that the equilibrated ordinary chondrites (EOC, or petrographic type 4–6 ordinary chondrites) are relatively altered by parent body metamorphism, while the unequilibrated ordinary chondrites (UOC, or petrographic type 3 ordinary chondrites) are least altered by parent body metamorphism.

The relationship between ordinary chondrites and S asteroids is a subject with a long and somewhat tortuous history. While Gaffey and cowriters (Gaffey et al. 1993, 2002; Gaffey 2007; Sunshine et al. 2004) argue that many

[1]Throughout this paper, we use the word "peak" for individual, essentially Gaussian, features that are actually absorptions, i.e., inverted peaks, and we use the word "band" for collections of peaks that appear as a single broad absorption feature observed in the spectrum. The presence of peaks in a band can often be resolved with the naked eye as inflections, bumps, or protruding peaks, but are sometimes completely unresolvable to the naked eye and require the help of analytical software like the MGM program. The assumption is that peaks can be assigned to specific sites and absorption mechanisms in the mineral. We think these definitions are in line with common usages.

of the S asteroids are melts or partial melts, other researchers argue that some or many of the S asteroids are related to ordinary chondrites and that past perceived differences (essentially the slope of the continuum) are due to alteration of the asteroid surface by space exposure, i.e., "space weathering" (Binzel et al. 1993, 2004; Chapman 1996). Of course both options can be true and taxonomy is a step toward clarifying this question.

In this article, we report new near-IR spectra for nearly 30 S complex asteroids representing most asteroid classes mentioned above and we compare them with the ordinary chondrites, especially the unequilibrated ordinary chondrites. The reason for our particular interest in the unequilibrated ordinary chondrites is that (1) being particularly unaltered by parent body processes, they are especially important in understanding solar system history; (2) they would lay on the surface of an asteroid that had either (a) an onion skin structure with unheated material on the surface and heated material inside, or (b) formed too late for any internal heating by ^{26}Al; (3) they have not been considered in any detail in the past. (Thermal models for the interiors of asteroids in relation to petrographic type have been published by McSween and Bennett [1996] and Akridge et al. [1998].) We tried to make quantitative comparisons by using the methods described above (the BAR plot and the MGM method). We conclude that many or most of the S(IV) asteroids have surfaces resembling UOC and we discuss some implications of this for asteroid history and internal structure. Progress reports of this work have appeared as conference abstracts (Gietzen et al. 2006, 2007, 2008, 2009; Gietzen and Lacy 2007; Sears et al. 2008), which are superseded by the present paper.

METHOD

Our asteroid spectra were obtained by using the NASA IRTF telescope on Mauna Kea, HI between August 6, 2004 and April 18, 2008 (Table 1). The classifications of these asteroids are listed in Table 2. The SpeX infrared spectrometer (Rayner et al. 2003) was used in the low-resolution prism mode, which yielded usable spectra for asteroids as faint as magnitude 17.5. The spectra covered the range 0.8–2.5 μm with a resolution element of 5 nm. The raw data were reduced using IRAF and IDL software. Data reduction included elimination of instrumental and atmospheric artifacts, normalization to solar analog spectra, and production of 1-dimensional wavelength-calibrated spectra. Our spectra are available at the project web site (http://www.uark.edu/misc/clacy/SpeX_site/index.htm/).

Since most of the asteroids observed had a broad absorption band at 1 μm that extended outside IRTF range, we spliced in visible spectra from the Small Main Belt Asteroid Spectroscopic Survey database (http://smass.mit.edu/smass.html).

To produce the BAR plot described by Gaffey et al. (1993a), the band area for each spectrum was calculated by using ORIGIN analysis software (by OriginLab Corp.). For the 1 μm absorption band, the area under the spectral curve between 0.7 and 1.4–1.7 μm region were determined by integration, subtracting the area under a continuum line between the same wavelength limits. The same procedure was applied to the 2 μm absorption band with an interval between 1.4–1.7 and 2.4 μm. The centers of the 1 μm band were determined by the method of Gaffey et al. (1993a). Reflectance values at each point on the continuum line were divided by the reflectance values for the observed spectrum and the trend of ratio versus wavelength described by a 3–8th order polynomial. The band center was then determined to be the center of the polynomial at one third of the reflectance at 1.4–1.7 μm. We checked the reliability of our methods by comparing selected results with those of Gaffey et al. (1993a).

The MGM software was obtained from the RELAB website and run using starting parameters similar to those reported elsewhere (e.g., Klima et al. 2007, 2011; their table 3). Over the 3 yr of this project, the spectra were analyzed many times with a variety of starting parameters but—for the major peaks especially—the results were essentially the same. This is no surprise, since most of the major peaks could be resolved by eye. Convergence was reached after three or four iterations (as was found by Sunshine and Pieters 1993). As we show below, the curves are generally well-fitted with only four or five peaks.

The MGM method allows the determination of the relative proportions of clinopyroxene to orthopyroxene. The uncertainty in these determinations for the present study was estimated to be ±7% by running the MGM analysis for multiple simulated spectra in which data were allowed to fluctuate randomly within a one-sigma level of the observed spectrum (the one-sigma level being determined by the counting statistics). This compares with ±10% found by Kanner et al. (2007) for Martian meteorites (in which considerable plagioclase is also present) using OMEGA spectra for Mars meteorites and the Martian surface.

The basis of our interpretation of these asteroid spectra was an analysis of the visible and near-IR spectra of a number of ordinary chondrites. We obtained spectra for these meteorites from the online databases (mainly PDS and RELAB) and we determined BAR parameters (Table 3) and performed MGM analyses (Table 4), using the methods described above for asteroids.

Table 1. Observational details for the present asteroids*.

Asteroid number	Asteroid name	UT Date	Exposure (s)	Airmass	Visual magnitude	Sky conditions	Analog stars	Phase angle (degrees)
6	Hebe	4/14/2005	320(12)	1.02	9.9		8,9,11	6.9
18	Melpomene	4/14/2005	160(16)	1.18	10.9		8,9,11	21.9
42	Isis	4/18/2008	960(32)	1.02	11.9	c,m	5,6,8	12.7
63	Ausonia	5/30/2006	480(16)	1.36	10.4		7,8,9,11	15.3
167	Urda	4/14/2005	480(8)	1.18	12.9		8,9,11	2.9
180	Garumna	1/22/2008	1440(12)	1.01	13.5	m	2,3,5,7	15.6
234	Barbara	4/27/2007	960(8)	1.02	14.4	m	6,7	18.7
246	Asporina	1/22/2008	1440(12)	1.09	13.1	m	2,3,5,7	13.3
269	Justitia	4/14/2005	1440(10)	1.23	13.1		8,9,11	25.2
349	Dembowska	1/22/2008	360(12)	1.01	10.5	m	2,3,5,7	18.0
354	Elonona	5/30/2006	640(16)	1.02	10.7		7,8,9,11	17.2
1036	Ganymed	5/30/2006	960(8)	1.14	14.3		7,8,9,11	14.5
1620	Geographos	1/22/2008	2880(24)	1.01	15.8	m	2,3,5,7	29.4
1980	Tezcatlipoca	12/29/2006	960(8)	1.12	14.6	m	3,4,5	24.7
2212	Hephaistos	12/29/2006	1920(16)	1.14	15.4	m	3,4,5	14.1
3288	Seleucus	1/22/2008	2880(24)	1.06	15.8	m	2,3,5,7	9.8
3908	Nyx	12/3/2004	1920(16)	1.01	15.3		1,2,5,6	38.4
4450	Pan	1/22/2008	2880(24)	1.02	16.2	m	2,3,5,7	18.7
4954	Eric	1/22/2008	300(20)	1.37	13.5	m	2,3,5,7	46.9
22771	1999CU3	10/14/2005	2880(24)	1.12	16.3	m	2,3,13	28.9
66251	1999GJ2	10/14/2005	960(8)	1.11	15.2	m	2,3,13	3.9
68950	2002QF15	5/30/2006	2880(24)	1.03	14.7		7,8,9,11	45.7
152895	2000CQ101	4/27/2007	2880(24)	1.06	16.3	m	6,7	35.1
170891	2004TY16	1/22/2008	2880(24)	1.09	15.6	m	2,3,5,7	35.1
152756	1999JV3	5/30/2006	2880(24)	1.00	16.6		7,8,9,11	34.9
143947	2003YQ117	5/30/2006	2880(24)	1.05	15.9		7,8,9,11	20.2
	2005NB7	4/18/2008	3840(32)	1.32	15.0	c,m	5,6,8	82.8

*Digital files of the spectra can be found at the following website (http://www.uark.edu/misc/clacy/SpeX_site/index.htm).

Exposure = The total exposure time, in seconds, followed by the number of CCD images (in parentheses) that were combined to produce the total exposure time.

Airmass = Mean airmass of the observations, calculated from the airmass values recorded at the start of each exposure.

Visual magnitude = Calculated visual (V-band) magnitude of the asteroid at the time of the observation.

Sky conditions = Sky conditions at the time of the observation, where c is for cloudy, roughly defined as the presence of clouds that led to erratic variations (greater than 5%) in the observed flux of either the solar-analog star or the asteroid; h is for a relative humidity greater than 70%; and m is for moonlight, where the lunar illumination is greater than 50%, and the moon's altitude above the horizon is greater than 20°.

Analog stars = The solar-analog star used in the calibration of the asteroid spectrum. 1: Land 92-276; 2: Land 93-101; 3: Hyades 64; 4: Land 97-249; 5: Land 98-978; 6: Land 102-1081; 7: Land 103-487; 8: Land 105-56; 9: Land 107-684; 10: Land 107-998; 11: Land 110-361; 12: Land 112-1333; 13: Land 113-276; 14: Land 115-271.

Phase angle = The angle between the Sun, the asteroid, and the Earth at the time of observation.

RESULTS

Our asteroids' near-IR spectra are shown in Fig. 1, with the SMASS data for the visible region spliced in. In the few cases where the SMASS database included IR data, they are also shown. For asteroids for which published classifications are available, the spectra are as expected for objects of that classification. For asteroids for which classifications were available, we were able to assign classifications. Thus we were able to assign Gaffey et al. (1993a) classifications to several S and S-like asteroids that previously had only Tholen-Bus-DeMeo classifications (DeMeo et al. 2009).

The asteroids we observed showed considerable diversity from V asteroid 3908, with its deep 1 and 2 μm bands characteristic of pyroxene-plagioclase-rich asteroids, to the pyroxene-olivine-rich S asteroids, with both bands generally shallower than the V asteroid and of various relative intensities, to finally the olivine-rich asteroids with no 2 μm band. Three examples are shown at greater resolution in Fig. 2. As expected, all asteroids had a steep slope in the UV and most had a positive continuum through most of the spectrum.

Because the basis of our interpretation of our asteroid spectra will be an analysis of ordinary chondrites, we begin by discussing their spectra. Since

Table 2. Taxonomy for the present asteroids.

Asteroid number	Asteroid name	Taxonomy[b] Gaffey	Tholen	Bus	DeMeo[c]
6	Hebe	S(IV)	S	S	S
18	Melpomene	S(V)	S	S	S
42	Isis	S(I)	S	L	K
63	Ausonia	S(II-III)	S	Sa	Sw
167	Urda	S(VI)[a]	S	Sk	Sw
180	Garumna	S(VI)[a]	S	Sq	Sr
234	Barbara	–	S	Ld	L
246	Asporina	S(I)[a]	A	A	A
269	Justitia	–	–	Ld	D
349	Dembowska	S(V)[a]	R	R	R
354	Eleonora	S(I)	S	Sl	A
1036	Ganymed	S(VI–VII)	S	S	Sr
1620	Geographos	S(IV)[a]	S	S	Sqw
1980	Tezcatlipoca	S(IV)[a]	SU	Sl	Srw
2212	Hephaistos	S(IV)[a]	SG	–	Sq:
3288	Seleucus	S(IV)[a]	S	K	Sw
3908	Nyx	–	V	V	V
4450	Pan	–	–		Sr:
4954	Eric	S(VI)[a]	–	S	Sr
22771	1999 CU3	–	–	Sl	Sw
66251	1999 GJ2	–	–	S[a]	Sr:
68950	2002 QF15	–	–		Sr:
152895	2000 CQ101	S(V)[a]	–	–	Q:
170891	2004 TY16	S(V)[a]	–	–	Sq:
152756	1999 JV3	S(IV)[a]	–	S	S
143947	2003 YQ117	–	–		S:
2005 NB7	2005 NB7	–	–		Sq:

[a]Assignments based on present work.
[b]Literature assignments: Gaffey et al. (1993a), Bus and Binzel (2002), Tholen (1989), and DeMeo et al. (2009).
[c]Assignments based on present work utilizing classification software from SMASS (smass.mit.edu/busdemeoclass.html). Classification of four asteroids (1036, 1980, 1620, and 22771) determined this way deviated from those reported in DeMeo et al. (2009).
"–" data not available; "na" method not applicable.

the mineralogy of these chondrites is well known, they provide ground truth from which we can use the asteroid spectra to discuss the compositions of their surfaces.

Analysis of Spectra for Unequilibrated and Equilibrated Ordinary Chondrites

The BAR Method

In Fig. 3, we plot the ten unequilibrated ordinary chondrites listed in Table 3 on the BAR plot of Gaffey et al. (1993a). Figures showing ordinary chondrites on this plot can be found in Gaffey (1976). All but two of the present UOC plot in the S(IV) field, only one (Bishunpur) is significantly outside. It is not clear why Bishunpur is outside the S(IV) field.

Running through the diagram in Fig. 3 is a heavy curve that connects olivine-rich objects (S(I)) with pyroxene-rich objects (S(VII)). Along this "mixing line" is class S(IV) in which the equilibrated and unequilibrated ordinary chondrites plot, suggesting that they are a more-or-less equal mix of the two minerals. In fact, Gastineau-Lyons et al. (2002) have shown that the chemical classes of equilibrated ordinary chondrite, the H, L, and LL classes, are resolvable within this field because differences in the olivine-pyroxene ratio are caused by their differences in oxidation state (e.g., Sears et al. 1996). Unequilibrated ordinary chondrites are not resolved on this plot, presumably because of their heterogeneity. It is often difficult to distinguish L3 chondrites from LL3 by any means.

The MGM Method

The results of our MGM analysis of ordinary chondrites are shown in Fig. 4 and Table 4. For the UOC, the software identified six peaks with centroids at about 0.4 (which was often only partially present), 0.9, 1.0, 1.2, 1.9, and 2.3 μm. For the EOC, the software identified peaks at 0.4 (which was often only partially present), 0.9, 1.0, 1.2, and 1.9 μm. Conspicuously absent from the EOC spectra is the peak at 2.3 μm, which in the UOC is large and broad and such strong influence on the spectra that the difference is apparent to the naked eye. We stress that while EOC and UOC spectra were run

Table 3. Unequilibrated ordinary chondrite meteorites used in the present study and their BAR parameters*

Chondrite	Type	Band I center	Band I area	Band II area	Band II/Band I
Tieschitz	H3.6	0.96	47.9	30.0	0.63
Dhajala	H3.8	0.96	39.6	26.6	0.67
Mezoe-Madaras	L3	0.96	5.5	4.4	0.80
Chainpur	LL3.4	0.94	3.7	2.2	0.59
Parnellee	LL3.6	0.95	11.3	7.4	0.65
Krymka	LL3.0	0.97	54.8	30.8	0.56
Dimmit	H3	0.98	33.5	10.2	0.30
Hedjaz	L3.7	0.96	10.4	5.2	0.50
Gorlovka	H3	0.96	11.8	10.1	0.86
Bishunpur	LL3.1	1.02	24.5	1.6	0.07

*Experimental uncertainties for individual spectra were not determined but based on the spectra for meteorites of the same class are assumed to be approximately 10% at the 2σ level.

Table 4. MGM parameters for ordinary chondrite meteorites determined in the present study.*

Meteorite	Peak 1		Peak 2		Peak 3		Peak 4		Peak 5		Peak 6	
	λ	d	λ	d	λ	d	λ	d	λ	d	λ	d
Equilibrated ordinary chondrites												
Bruderheim	0.4	−0.13	0.87	−0.2	1	−0.26	1.23	−0.1	1.92	−0.22	–	–
Colby (Wisc)	0.42	−0.22	0.88	−0.2	1.04	−0.28	1.27	−0.13	1.94	−0.12	–	–
Manbhoom	Present	< −0.7	0.87	−0.19	0.99	−0.44	1.23	−0.24	1.94	−0.14	–	–
Unequilibrated ordinary chondrites												
Bishunpur	0.45	−0.18	0.93	−0.05	1.05	−0.07	1.3	−0.04	1.82	0.02	2.28	−0.02
Dhajala	Present	< −0.10	0.88	−0.07	0.96	−0.17	1.23	−0.14	1.87	−0.24	2.46	−0.2
Hedjaz	Present	< −0.40	0.89	−0.1	1.03	−0.09	1.29	−0.07	1.92	−0.12	2.4	−0.07
Parnallee	Present	< 0.7	0.87	−0.15	1	−0.22	1.26	−0.07	1.92	−0.23	2.41	−0.2
Tieschitz	Present	< −0.7	0.87	−0.13	1	−0.18	1.23	−0.13	1.93	−0.19	2.43	−0.07

*Peaks in the reflectance spectra of ordinary chondrites identified by the MGM method, their wavelength (λ, μm), and depth (d). Uncertainties (2σ): Centroid ±0.01 μm; depth ±0.02.

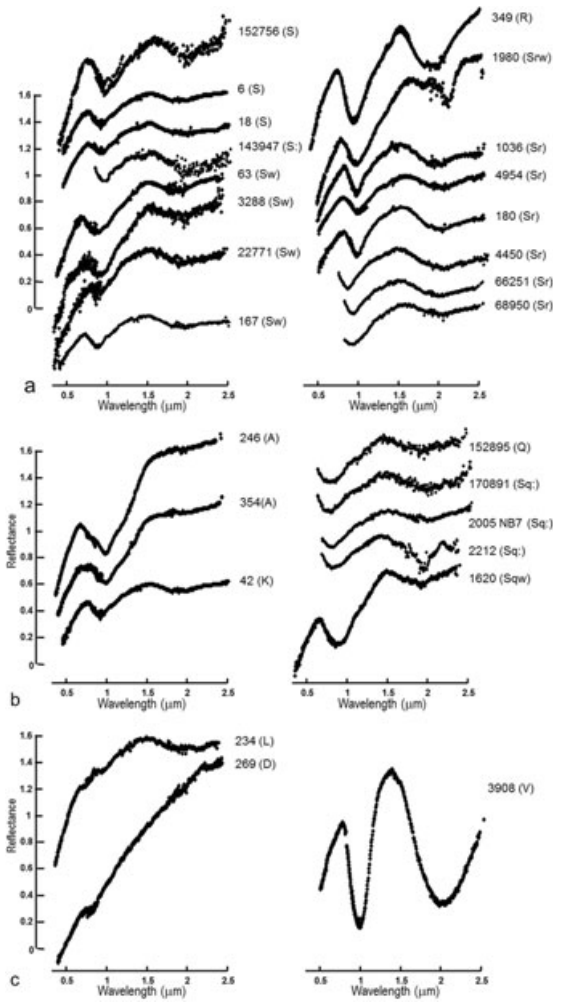

Fig. 1. Spectra for the S complex asteroids reported in this paper. The data over the 0.8–2.5 μm range were obtained by the authors by using NASA's IRTF and SPEX spectrometer, augmented by data over the visible range obtained from the online databases (Xu et al. 1995; Binzel et al. 2001, 2004; Bus and Binzel 2002). a) S asteroids (except Sq). b) A, K, Sq, and Q asteroids. c) V, L, and D asteroids.

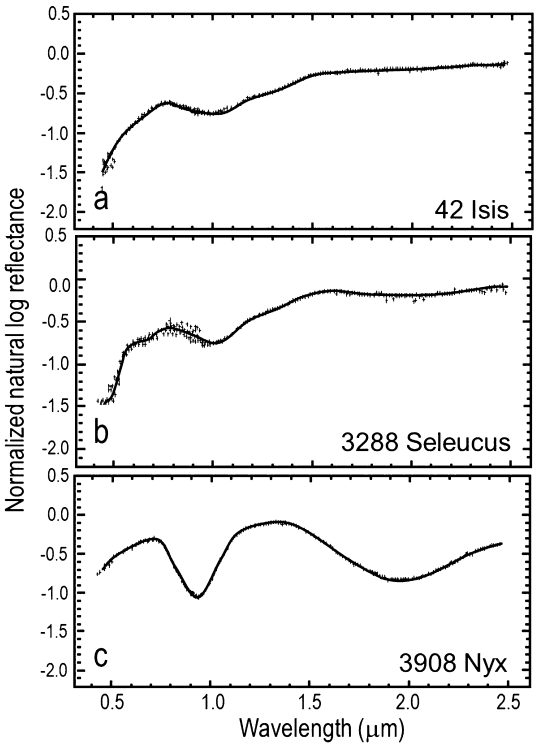

Fig. 2 Spectra for three asteroids from the present study representing the series olivine-rich (a, asteroid 42 Isis), olivine- and pyroxene-rich (b, asteroid 3288 Seleucus), and pyroxene- and plagioclase-rich (c, asteroid 3908 Nyx). The approximately 2 μm pyroxene band (Band II) is weak or absent in the 42 Isis spectrum, while it is very strong in the spectrum of 3908 Nyx. The intermediate case, asteroid 3288 Seleucus, shows both Band I (about 1 μm) and Band II reflecting the presence of both olivine and pyroxene.

multiple times with slight variations in starting parameters used for the MGM analysis, this difference persists. Figure 5 provides a visual representation of the peak positions (excluding the 2.3 μm peak) given in Table 4.

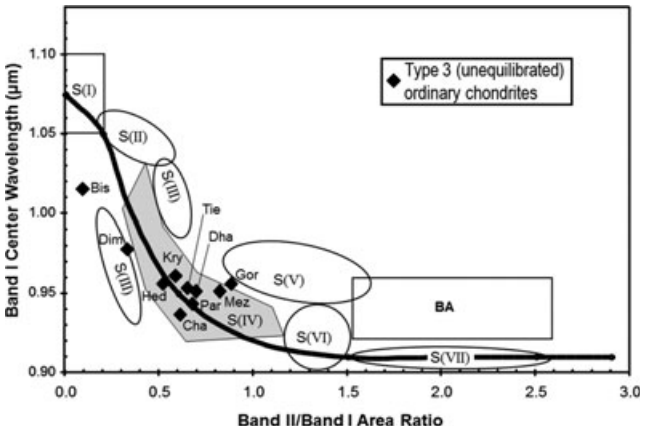

Fig. 3. Wavelength of the center of approximately 1 μm absorption band (Band I) against the ratio of the area under the 2 μm band (Band II) to the area under the 1 μm band (the "BAR plot") which Gaffey et al. (1993a) use to define eight groups of S complex asteroids, S(I) to S(VII), and also indicating the position of basaltic achondrite (BA) meteorites. Plotted on this figure are data for ten type three ordinary chondrites (also known as unequilibrated ordinary chondrites, or UOC). All but two plot in the S(IV) field in which equilibrated ordinary chondrites (EOC) plot. The meteorites are identified by their first three letters, Bishunpur, Dimmitt, Hedjaz, Krymka, Tieschitz, Dhajala, Chainpur, Parnallee, Mezö-Madaras, and Gorlovka. Data are obtained from the Planetary Data System (mainly from Gaffey 1976).

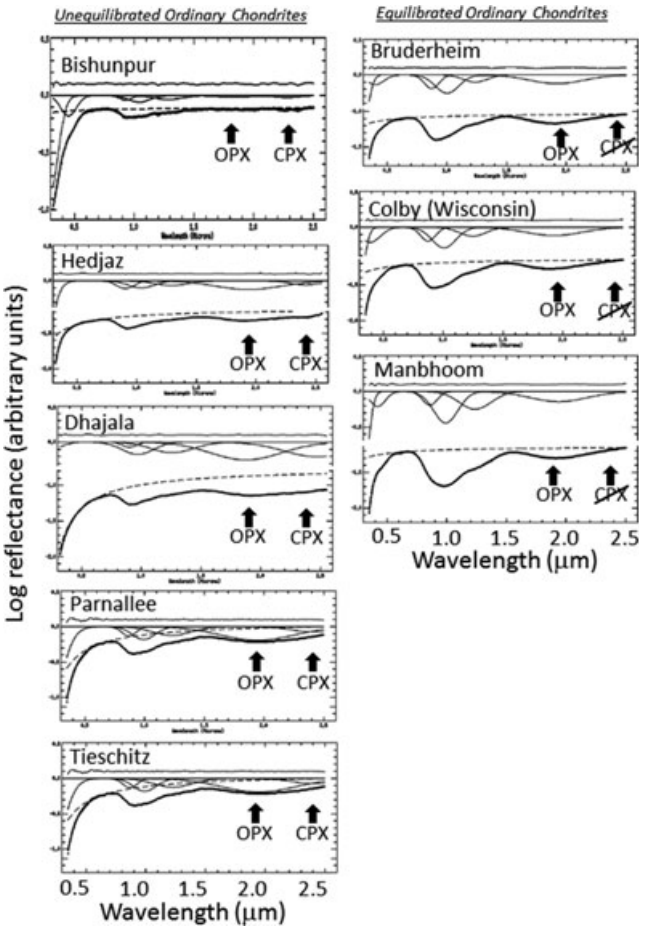

Fig. 4. Sketches of the spectra of five unequilibrated ordinary chondrites and three equilibrated ordinary chondrites with the individual Gaussian peaks identified by the MGM method indicated. The curves are fitted with four or five Gaussian peaks with no significant residuals. As expected on the basis of petrographic observations, spectral analysis suggests that the UOC are free of clinopyroxene (CPX) while the EOC contain both CPX and orthopyroxene (OPX). The data sources as in Fig. 3. CPX crossed through indicates the expected position of the peak characteristic of CPX.

These results are consistent with the known mineralogy of these ordinary chondrites. They are mainly a mixture of olivine and pyroxene with lesser amounts of plagioclase, metal, and sulfide. As mentioned above, what distinguishes the UOC from the EOC is the structural state of the pyroxene. There is a small amount of calcic pyroxene (diopside) in both UOC and EOC, but most of the pyroxene in ordinary chondrites is Ca-poor. As stated above, but worth stressing, in the UOC half or more of the pyroxene is in the clinopyroxene form, while in the EOC all the Ca-poor pyroxene is orthopyroxene. Parent body metamorphism causes conversion of CPX to OPX along with recrystallization, coarsening, chemical homogenization, and destruction of chondrule textures. Diopside changes little during metamorphism, besides coarsening a little.

Literature data for peak assignments are in agreement with the attribution of the 1.0 μm peak to orthopyroxene and the 2.4 μm peak to clinopyroxene, recognizing that in most previous studies the CPX is calcium-rich (e.g., Kanner et al. 2007) and the Ca-poor pyroxene is orthopyroxene (e.g., Klima et al. 2011).

To check our interpretation that the 2.3 μm peak in UOC is due to low-Ca CPX known to be present in these meteorites, we requested six Ca-poor clinopyroxenes from the Smithsonian Institution and obtained those listed in Table 5. We also obtained compositional data from the literature (essentially the references quoted in Deer et al. 1996; and the MinDat online database). We obtained our own spectra using a Nicolette FTIR instrument (see Gietzen et al. [2009] for an example of a spectrum), but we also arranged for measurements to be made at Brown University by Takahiro Hiroi. Essentially the same spectra were obtained by both laboratories. Our Ca-poor CPX spectra were weaker than the meteorite spectra because of sometimes considerable amounts of weathering products, and the spectra sometimes showed bands attributable to trace amounts of water. We tried to remove the water by heating in an oven at 110 °C overnight and by acid washing (3 M HCl for 10 min). While these treatments

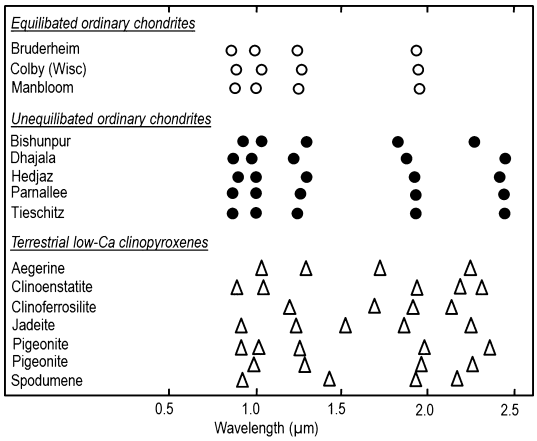

Fig. 5. Positions of individual Gaussian peaks located by the MGM software for EOC, UOC, and terrestrial low-Ca clinopyroxenes. Scatter on the data for terrestrial samples reflect the presence of weathering products which could not be entirely removed by heating or acid treatment. Notwithstanding this problem, the three sets of samples have very similar suite of peaks, the exception being the lack of the CPX peak at 2.3–2.5 μm in the EOC. Petrographic studies indicate that the EOC are CPX-free.

considerably reduced the depths of the water bands, a few water bands remained, but they were very small and could be removed using the MGM software. Other effects of weathering, such as a reddening of the spectra, are allowed for in continuum fitting and do not affect the analysis of the peaks.

In Table 6, we list the peaks identified by the MGM software and in Fig. 5 we also show the peaks that the MGM software located in the terrestrial low-Ca CPX. There is more scatter in the terrestrial data than the meteorite data because of the weakness of the terrestrial spectra and the presence of weathering products, but clearly four of the five major peaks in UOC are present in the terrestrial CPX and the peak at 1.0 μm in the terrestrial CPX might be resolvable into 0.9 and 1.0 μm peaks with better data. The peaks at approximately 1.5 μm in clinoenstatite and jadeite are probably due to an unrecognized water peak. We are very confident in arguing that the distinction between the UOC and EOC spectra is caused by the structural form of the low-Ca pyroxene and that UOC and EOC have significantly different near-IR spectra. We compare our new data for Ca-poor clinopyroxenes with the data from the Klima et al. (2011) in Fig. 6. This supports our contention that it is structure and not composition that primarily determines the position of the approximately 2 μm band. Most of the CPX in Fig. 6 have bands at about 2.3 μm regardless of their composition.

Analysis of Spectra for S Asteroids

The BAR Method

Our data for the present asteroids are plotted on the BAR plot in Fig. 7, omitting asteroids with no data in the visible range for which accurate centroids cannot be determined. Figure 7a shows the fields defined by Gaffey et al. (1993a). Our present suite of asteroids plot across the whole diagram, from the olivine-rich S(I) asteroid 246 to the V asteroid 3908 (Fig. 7b). A large fraction of our asteroids plot in the S(IV), S(V), and S(VI) fields. Within the limits of the statistics of small numbers, this distribution of S asteroids over the seven subclasses is similar to that of Gaffey et al. (1993a).

These data provide an opportunity to compare taxonomic schemes (Table 2). Since both the Bus and Tholen schemes are based on spectral shape in the visible range, and Bus et al. (2002) attempted to absorb the Tholen classes into their scheme, it is not surprising to see a broad level of agreement. Similarly, the incorporation of near-IR spectra into the classification scheme did not significantly change the situation (DeMeo et al. 2009). Figure 7c identifies the asteroids on the BAR plot and the Gaffey et al. (1993a) classes S(I)–S(VII) in terms of their Tholen-Bus-DeMeo classifications as given by DeMeo et al. (2009). As expected, the class A asteroid and two Sl asteroids plot with the olivine-rich S(I) class and the V asteroid plots with the pyroxene-rich basaltic achondrite (BA) field. The Sw, Sqw, and Srw generally occupy the entire S(IV) region while S, Sr, and R asteroids approximately occupy the lower half of the S(IV) field. Thus, while the Tholen-based scheme is purely descriptive and the

Table 5. Terrestrial Ca-poor CPX minerals used in this study.*

Sample	Cat. No.	Source	Wo (wt %)
Aegerine	NMNH C2431	Quincy, Massachusetts	0.58
Clinoenstatite	NMNH 163346	Napoui, New Caledonia	~0
Clinoferrosilite	NMNH 145787	Ravensworth, New South Wales, Australia	~0
Jadeite	NMHN 113778	Clear Creek, California	5.57
Pigeonite	NMHN 105869	Hakone Volcano, Honshu, Japan	14.60
Spodumene	NMNH R3068	Etta Mine, South Dakota	0.23

*Samples were provided by the Mineral Science Department of the National Museum of Natural History (Smithsonian Institution) and their catalog numbers are given. Compositional data are taken from sources given in Deer et al. (1996) and the MinDat online database.

Table 6. RELAB spectra identifier and MGM parameters obtained for Ca-poor clinopyroxenes.[a]

Sample	RELAB ID	Wo (wt %)	Peak 1		Peak 2		Peak 3		Peak 4		Peak 5		Peak 6		Peak 7	
			λ	d	λ	d	λ	d	λ	d	λ	d	λ	d	λ	d
Aegerine	PX-DWS-013	0.58			1.05	−0.05	1.3	−0.2	1.74	−0.08	2.23	−0.03				
	PX-DWS-013-B[c]															
Clinoenstatite	PX-DWS-016	∼0			0.9	−0.18	1.06	−0.08	1.93	−0.07	2.2	−0.03	2.32	−0.02		
	PX-DWS-016-A[b]															
	PX-DWS-016-AB[d]															
	PX-DWS-016-B[c]															
Clinoferrosilite	PX-DWS-011	∼0					1.2	−0.1	1.69	−0.05	1.92	−0.05	2.17	−0.04	> 2.5	< −0.1
	PX-DWS-011-A[b]															
	PX-DWS-011-AB[d]															
	PX-DWS-011-B[c]															
Jadeite	PX-DWS-015	5.57			0.9	−0.5	1.22	−0.37	1.52	−0.24	1.86	−0.17	2.23	−0.08		
	PX-DWS-015-B															
Pigeonite	PX-DWS-012	14.6	0.47	−0.3	0.9	−0.04	1	−0.12	1.25	−0.03	1.98	−0.08	2.35	−0.04		
	PX-DWS-012-B[c]															
Spodumene	PX-DWS-014	0.23			0.93	−0.02	1.44	−0.04	1.94	−0.04	2.19	−0.06				
	PX-DWS-014-A[b]															
	PX-DWS-014-AB[d]															
	PX-DWS-014-B[c]															

[a]Peaks in the reflectance spectra of ordinary chondrites identified by the MGM method, their wavelength (λ, μm) and depth (d, natural log units). Uncertainties (2σ): Centroid ±0.05 μm; depth ±0.02. Spectra were also obtained at the University of Arkansas in good agreement with the RELAB spectra.

[b]Dried in air at 105 °C for 24 h.

[c]Washed with HCl and dried at 120 °C.

[d]Dried at 105 °C 24 h, washed with HCl & dried at 120 °C.

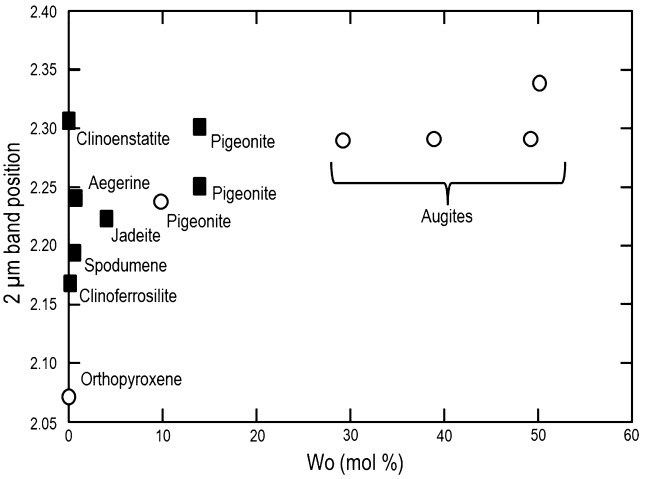

Fig. 6. Plot comparing the position of the approximately 2 μm peak with the calcium content of pyroxenes. The figure is based on fig. 9 of Klima et al. (2011) whose data are shown as open symbols. Augite, pigeonite, jadeite, clinoferrosilite, and clinoenstatite are CPX. Data for CPX obtained in the present study are shown as filled symbols. Contrary to the earlier workers, we argue that the position of this peak is determined by the structure of the pyroxene rather than its composition, CPX having peaks >2.15 μm, OPX having peaks <2.15 μm.

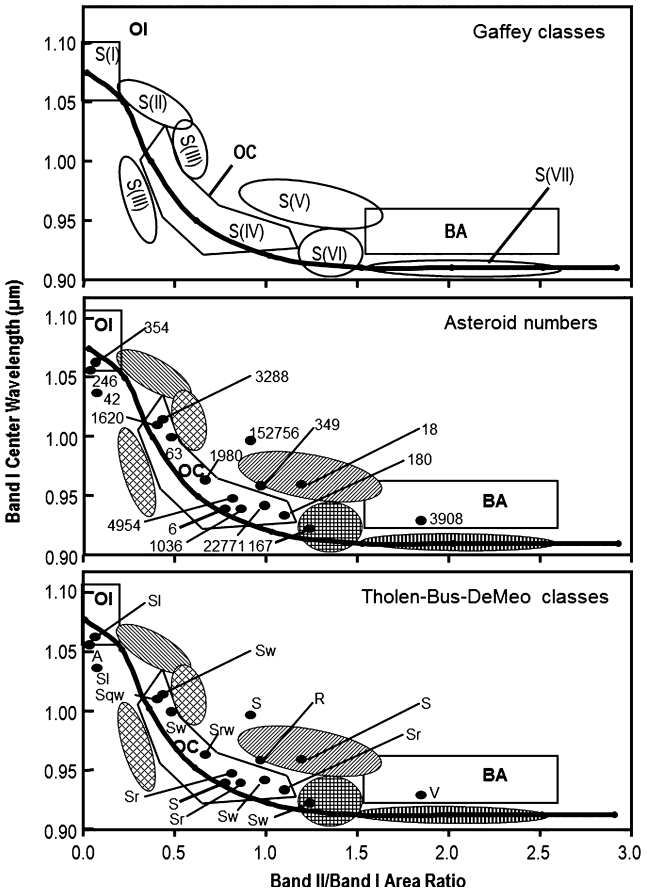

Fig. 7 The BAR plot showing a) eight groups of S complex asteroids, S(I) to S(VII), plus the region identified with the basaltic asteroids (BA), as defined by Gaffey et al. (1993a). A line passing through the fields is an olivine (top left)—pyroxene (bottom right) mixing line. Olivine-rich objects plot at the left of the trend (Ol); pyroxene-rich asteroids plot at the right end of the trend; ordinary chondrites (OC), which are mixtures of olivine and pyroxene, plot in the middle. b) Distribution of the present asteroids (where the appropriate data are available) identified by asteroid number. c) Distribution of 12 of the present asteroids on this plot identified by their DeMeo et al. (2009) classifications illustrating a broad level of agreement between the DeMeo and Gaffey schemes.

BAR-based scheme is intended to be mineralogical, the two classification schemes are in broad agreement.

For the purposes of this article, we conclude from Fig. 7 that many of the present asteroids plot in the S(IV) field, where the ordinary chondrites and, most importantly, the unequilibrated ordinary chondrites have also been observed.

The MGM Method

A spectral analysis by the MGM method was performed on all asteroid spectra for which we could locate data in the visible region (Table 7), and which had measurable bands in the 1 μm region (olivine) or both the 1 and 2 μm regions (pyroxene). Figure 8 shows the spectra of three asteroids, one from each end of the mixing line and one from the middle, illustrating the results of the curve fitting. The mineralogical differences in the surfaces of these asteroids are readily apparent from these results. Olivine has major bands that MGM can locate at about 0.88, 1.06, and 1.25 μm, depending on Fe content. In the absence of pyroxene, as in the case of S(I) asteroids, these peaks dominate the spectra. One example is asteroid 42 Isis (Fig. 8a). Pyroxene bands are strong in the spectra of V asteroids like asteroid 3908 (Fig. 8c). Olivine and pyroxene are apparent in the combination of absorption bands from most S complex asteroids, the example shown being asteroid 3288 (Fig. 8b).

In Fig. 9, we show the locations of the peaks identified by the MGM program in the spectra for the present asteroids for which we have Gaffey et al. (1993a) classifications. Considering the diversity in the spectra, and that the MGM program was run multiple times over many years with slightly different starting parameters, the peaks identified are remarkably consistent, as are the differences. The spectra can be resolved into as few as five and as many as six individual peaks, seven for 4954 Eric, which has a peak at 1.45 μm. For the rest of the spectra, there are peaks at 0.6, 0.8–0.9, 1.0–1.1, 1.2–1.3, 1.9, and 2.3 μm. The 0.6 and 2.3 μm peaks are not

Table 7. Asteroid observed for the present study for which MGM parameters were obtained.*

	Peak 1		Peak 2		Peak 3		Peak 4		Peak 5		Peak 6		Peak 7		Peak 8	
Asteroid	λ	d	λ	d	λ	d	λ	d	λ	d	λ	d	λ	d	λ	d
6 Hebe	< 0.4	< −0.4	0.66	−0.10	0.88	−0.20	1.04	−0.12	1.24	−0.08			2.30	−0.03		
7 Iris					1.05	−0.70	1.03	−0.24	1.76	−0.10	2.01	−0.02	2.23	−0.03		
18 Melpomene	< 0.4	< −0.4	0.65	−0.04	0.89	−0.10	1.05	−0.08	1.27	−0.04	1.86	−0.10	2.28	−0.08		
42 Isis	< 0.4	< −0.4	0.64	−0.09	0.87	−0.22	1.03	−0.30	1.24	−0.22	1.95	−0.03				
63 Ausonia	< 0.4	< −0.4	0.58	−0.47	0.86	−0.40	1.03	−0.36	1.27	−0.20	1.94	−0.12				
167 Urda	< 0.4	< −0.4	0.65	−0.12	0.88	−0.17	1.04	−0.10	1.23	−0.04	1.88	−0.07	2.26	−0.04		
180 Garumna	< 0.4	< −0.4	0.66	−0.26	0.92	−0.47	1.08	−0.13	1.23	−0.10	1.90	−0.22	2.42	−0.14		
234 Barbara 1	< 0.4	< −0.4	0.58	−0.37	0.83	−0.20	1.03	−0.14	1.23	−0.07	1.87	−0.04	2.23	−0.07		
246 Asporina	< 0.4	< −0.4	0.63	−0.07	0.87	−0.20	1.03	−0.32	1.24	−0.30						
269 Justitia			0.62	−0.52	0.87	−0.40	1.06	−0.30	1.32	−0.25	1.74	−0.12				
349 Dembowska	< 0.4	< −0.4	0.63	−0.3	0.92	−0.13	1.03	−0.64	1.26	−0.35	1.88	−0.58	2.35	−0.10		
354 Eleonora	< 0.4	< −0.4	0.65	−0.1	0.82	−0.14	1.02	−0.27	1.22	−0.24	2.02	−0.03				
1036 1 Ganymed	< 0.4	< −0.4			0.90	−0.20	1.02	−0.10	1.20	−0.05	1.88	−0.16	2.48	−0.13		
1036 2 Ganymed					0.90	−0.28	1.03	−0.14	1.22	−0.07	1.86	−0.12	2.36	−0.07		
1620 Geographos	< 0.4	< −0.4	0.61	−0.08	0.87	−0.24	1.02	−0.40	1.26	−0.20	1.95	−0.12	2.32	−0.08		
1980 Tezcatlipoca	< 0.4	< −0.4	0.66	−0.42	0.88	−0.97	1.03	−0.69	1.27	−0.37	1.87	−0.2	2.07	−0.27		
1999 JV3	< 0.4	< −0.4			0.92	−0.40	1.13	−0.32	1.39	−0.47	1.93	−0.68	2.39	−0.49		
2033 YQ117					0.92	−0.22	1.06	−0.12	1.27	−0.05	1.92	−0.13	2.27	−0.07		
2005 BN7					0.91	−0.34	1.03	−0.28	1.27	−0.14	1.90		2.28	−0.08		
2212 Hephaistos					0.88	−0.47	1.06	−0.40	1.28	−0.23	1.87	−0.12	2.06	−0.22		
3288 Seleucus	0.48	−0.62	0.52	−0.40	0.82	−0.27	1.02	−0.45	1.25	−0.25	1.89	−0.10	2.23	−0.07		
3908 Nyx	< 0.4	< −0.4			0.82	−0.20	1.16	−0.12			1.84	−0.70	2.13	−0.42	> 2.5	> −0.25
4450 Pan					0.92	−0.43	1.03	−0.27	1.25	−0.13	1.90	−0.23	2.22	−0.10	> 2.5	< −0.10
4954 Eric	< 0.4	< −0.4	0.64	−0.08	0.91	−0.47	1.07	−0.17	1.24	−0.10	1.94	−0.20	2.40	−0.09		
22771	0.38	−0.45	0.67	−0.17	0.88	−0.17	1.03	−0.13	1.25	−0.07	1.88	−0.09	2.27	−0.07		
68950					0.9	−0.22	1.03	−0.13	1.22	−0.07	1.90	−0.12	2.27	−0.06		
152895					0.89	−0.40	1.03	−0.38	1.25	−0.25	1.90	−0.17	2.27	−0.11		
170891					0.89	−0.28	1	−0.32	1.24	−0.32	1.88	−0.33	2.32	−0.3		

*Peaks in the reflectance spectra of the present asteroids identified by the MGM method, their wavelength (λ, μm), and depth (d). Uncertainties (2σ): Centroid ±0.01 μm; depth ±0.02.

present in all samples. Instead, the 0.6 μm peaks are sometimes missing in S(IV), S(V), and S(II, VII) asteroids and the 2.3 μm peak is missing in the S(I) and S(II, III) asteroids. In two S(IV) samples, the approximately 2.3 μm peak has been replaced by a peak at about 2.1 μm. It is the 2.3 μm peak that particularly interests us as it suggests the presence of clinopyroxene in all asteroid classes except S(I) and S(II, III).

Sunshine et al. (1990) and Sunshine and Pieters (1993) showed that it was possible to use the relative strengths of the CPX and OPX peaks, with laboratory calibration, to estimate the relative amounts of these two phases. The relative amounts of clinopyroxene and orthopyroxene based on the approximately 1 and 2 μm bands appear in Table 8 and are plotted in Fig. 10. While the estimates have large uncertainties, due to the presence of other mineral phases and variations in the Fe content of the pyroxene, there is a broad level of agreement between the estimates based on the 1 μm band and those based on the 2 μm band. There is no readily apparent relationship between position on the plot and asteroid class; it appears that we can assert that asteroids of all classes contain a mixture of CPX and OPX on their surfaces. There is even a suggestion of two clusters, about 50% and about 70%. The only type of ordinary chondrite meteorites containing significant amounts of CPX are the unequilibrated ordinary chondrites and these amounts are in reasonable agreement with petrographic estimates for the fraction of CPX-bearing chondrules in UOC (Rubin, personal communication).

DISCUSSION

We have obtained near-IR spectra for nearly 30 S and S-like (high albedo) asteroids including several near-Earth asteroids with the objective of relating them to meteorites, and in particular the ordinary chondrites and especially the type 3 (unequilibrated) ordinary chondrites. We therefore begin our discussion with a consideration of the effectiveness of reflectance spectroscopy in distinguishing equilibrated from unequilibrated ordinary chondrites. In this case, we have ground truth because

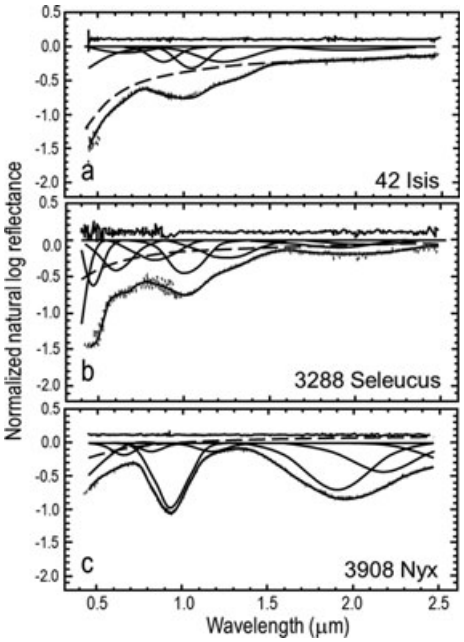

Fig. 8. The spectra shown in Fig. 2 with the results of the MGM analysis included. The approximately 2 μm pyroxene band (Band II) is weak or absent in the 42 Isis spectrum (a), while it is the very strong in the spectrum of 3908 Nyx(c). The intermediate case (b), asteroid 3288 Seleucus, shows both Band I (approximately 1 μm) and Band II reflecting the presence of both olivine and pyroxene. The spectra are shown as a series of plus signs with the results of deconvolution by the MGM software appearing as inverted approximately Guassian curves. The continuum is shown as a broken line. The sum of the modified Gaussian curves and the continuum is shown as a smooth line passing through the spectra generally indistinguishable from it. The residuals (difference between the sum and the spectrum data points) are displaced upwards by 10%.

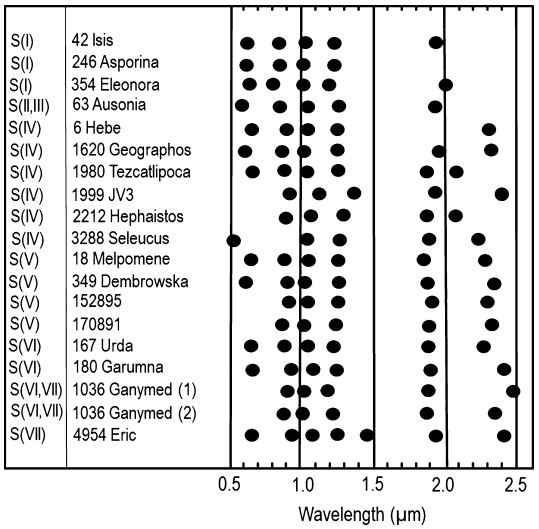

Fig. 9. Individual Gaussian peaks identified by the MGM software for the present asteroids for which Gaffey et al. (1993a) classes are known. All our asteroid spectra could be fitted with five to seven peaks with insignificant residuals. Four of the six ordinary chondrite–like S(IV) asteroids, and all of the S(V)–S(VII) asteroids, show evidence for a 2.3–2.5 μm peak characteristic of CPX. As expected the olivine-rich asteroids of classes S(I)–S(III) show no evidence for the 2.3–2.5 μm.

there are many decades of data on the mineralogy of ordinary chondrites and the differences in mineralogy between the EOC and the UOC. Having established this, we will discuss the S asteroids and their composition. Finally, we summarize the two together and discuss the implications of these data for the asteroidal sources of ordinary chondrites and the internal structure of comparable types of asteroid.

Reflectance Spectra of Equilibrated and Unequilibrated Ordinary Chondrites, Ca-Poor Clinopyroxenes, and Ground Truth

In our early attempts to compare ordinary chondrite spectra with our spectra for S asteroids we noticed that the UOC spectra often had a shallow dip at about 2.3 μm that was absent in the spectra for the EOC and that if there was no dip, the continuum appeared a little less steep for the UOC. This was confirmed when we applied the MGM method of spectrum analysis, as a peak at 2.3–2.5 μm was invariably located in the near-IR spectra of UOC but not in spectra of EOC (Fig. 4). While we did not keep a record of our starting parameters, we initially used starting parameters similar to those used in the literature (e.g., table 3 in Klima et al. 2007, 2011) and over the three or so years of this project used a variety of input parameters with essentially the same result. The

Table 8. Clinopyroxene estimates for the present asteroids for which this could be determined.*

		%CPX	
Asteroid number	Asteroid name	1 μm	2 μm
6	Hebe	53.0	30.5
18	Melpomene	69.5	71.5
63	Ausonia	81.0	53.0
167	Urda	49.0	46.5
180	Garumna	40.0	59.0
234	Barbara	60.5	70.5
349	Dembowska	51.0	18.0
1036	Ganymed	48.0	77.0
1980	Tezcatlipoca	61.5	75.0
3288	Seleucus	80.0	59.5
3908	Nyx	91.0	56.0
22771	1999 CU3	75.5	65.5
152756	1999 JV3	58.5	34.5

*Percentage of the pyroxene that is clinopyroxene as estimated using the MGM software (Sunshine and Pieters 1993). One-sigma uncertainties (see text for explanation) are typically 7%.

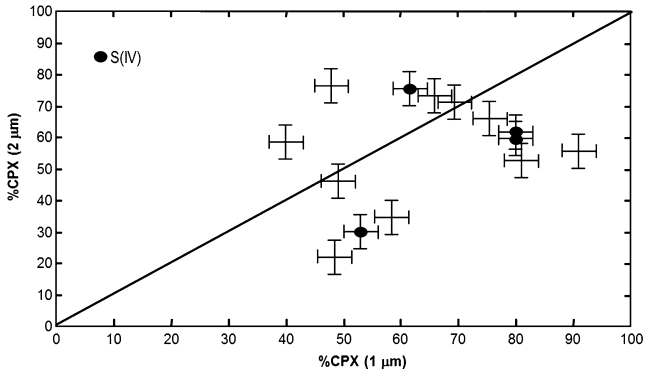

Fig. 10. Estimates based on the MGM analysis for the amount of clinopyroxene in the pyroxene as determined by the 1 μm band with the amount estimated using the 2 μm band. While there is scatter caused by the presence of other minerals, there is evidence for CPX in most of the asteroids in our study and that the amount of the pyroxene that is CPX is about 50%, in fact there is a suggestion of bimodality, with a cluster at 50% and another at 70%. Note that S(IV) asteroids appear in both clusters. The diagonal is a unity line.

conclusion that the 2.3 μm peak is present in UOC and absent in EOC is very robust, in our view.

It also seems well established in the literature that the 2.3 μm peak is due to clinopyroxene, frequently referred to as high-Ca pyroxene or HCP. This topic has a long history (e.g., Klima et al. 2007, 2011; Clénet et al. 2011; and references therein) and the effects of cation substitution have also been explored in some detail (e.g., Klima et al. [2011] and references therein). There is also a 0.9 μm peak due to clinopyroxene with similar properties to the 2.3 μm peak and both are offset to longer wavelengths relative to the corresponding orthopyroxene peaks at about 1.9 μm and about 0.8 μm. What we stress here is that there are the low-Ca clinopyroxenes with spectroscopic properties similar to the high-Ca clinopyroxenes (Figs. 5 and 6). Low-Ca clinopyroxenes are rare on Earth. Deer et al. (1996) list only a handful of natural occurrences, and one of their listed source locations is the UOC. On the other hand, in understanding the history of the largest meteorite class, the ordinary chondrites, the presence or absence of this phase is extremely important.

It was probably Dodd et al. (1967) who first observed that maybe half the low-Ca pyroxene in UOC was in the monoclinic form and that parent body metamorphism "equilibrated" these meteorites (homogenized mineral compositions, destroyed chondrule outlines, coarsened matrix, and metal, etc.) and converted the clinopyroxene to orthopyroxene. So important was the change in the pyroxene that it became part of the widely accepted and highly successful chondrite classification scheme of Van Schmus and Wood (1967).

Aside from the low-Ca pyroxene, there is a small amount (perhaps 5 vol%) of high-Ca (diopside) that coarsens during metamorphism but otherwise changes little. It is possible that a spectrometer with sufficient sensitivity and software with sufficient capability could detect the presence of high-Ca clinopyroxene in the near-IR spectrum of EOC, but the spectra will always be dominated by the orthopyroxenes.

Our "ground truth" is that UOC can be distinguished from EOC by their reflectance spectra by the presence of a strong peak at about 2.3 μm peak in the UOC spectra. Our interpretation, based on the literature and our spectra for Ca-poor clinopyroxenes, is that this reflects the presence of abundant clinopyroxene in UOC but not EOC. It is theoretically possible for an EOC to have a 2.3 μm peak due to the presence of diopside, but this phase is in minor amounts, and was not detected in the EOC spectra we analyzed.

The Nature of S Asteroid Surfaces

Gaffey et al. (1993b) have discussed in some detail the mineralogical implications of the BAR plot pointing out that the asteroid classes lie along a mixing line from olivine (top left) to pyroxene (bottom right). On the basis of the proposed mineralogy, these authors linked the classes to meteorite classes, virtually always to igneous classes. For example, they correlate S(I) with pallasites, S(II) with CPX-bearing ureilites, S(III) OPC-bearing ureilites, S(V) with lodranites, S(VI) with IAB irons, and S(VII) mesosiderites. Of the 27 mineral assemblages Gaffey et al. (1993b) thought could be associated with their seven classes, all but one possible mineral association represented melts or partial melts. Eleven of Gaffey et al. (1993b) asteroid classes are not represented among the world's meteorite collections (Gaffey et al. 1993, 2002; Gaffey 2007).

In addition, the field labeled BA in Fig. 11 corresponds to basaltic achondrites, an ambiguous term for the howardites, eucrites, diogenites meteorites, related to Vesta and the V asteroids (McCord et al. 1970; Feierberg and Drake 1980; Drake 2001; Cochran et al. 2004). These meteorites contain abundant high Ca clinopyroxene and plagioclase, so again these are igneous rocks, or breccias made by mixing various sorts of igneous rocks (Duke and Silver 1967; Buchanan and Reid 1996; Mayne et al. 2009).

The exception to the general statement that the fields on the BAR plot represent asteroids whose surfaces are melts or melt products was the Gaffey et al. (1993b) suggestion that S(IV) may be analogous to ordinary chondrites. This class seems to correspond to mixtures of olivine (OL) and orthopyroxene with OPX (OPX + OL) values between 0.2 and 0.5. This is consistent with the

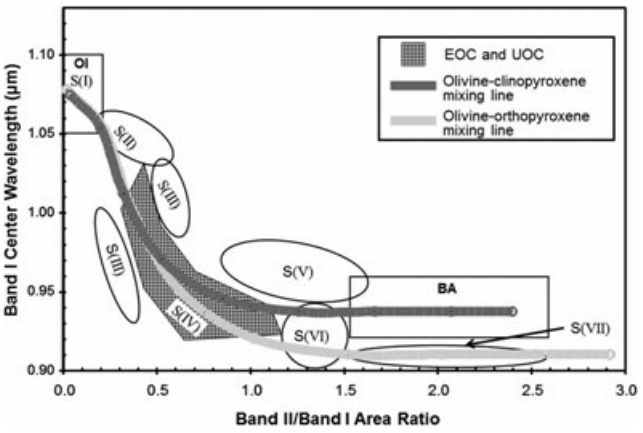

Fig. 11. The BAR plot with two mixing lines indicated. The lower line is the line suggested by Gaffey et al. (1993a) and thought to represent the mixing of olivine and orthopyroxene. We suggest that this is the mixing line between olivine and low-Ca pyroxene. The upper line is the same line pinned at olivine end and adjusted upwards at the pyroxene end to pass the monoclinic, high-Ca pyroxene. This upper line refers to the olivine-clinopyroxene mixing. However, all the asteroids in the present study and the UOC that plot in the S(IV) field contain a mixture of orthopyroxene and clinopyroxene, so the lower line reflects the presence of orthopyroxene rather than being pure orthopyroxene.

mineral assemblages found in OPX-rich ureilites, lodranites, winoites, IAB irons (all igneous rocks), or—and this is especially important for the present paper—the ordinary chondrites. As we have seen, EOC and UOC plot in the S(IV) field (Table 3; Fig. 3).

In a minor extension of a suggestion of Gaffey et al. (1993a), we suggest that there are two mixing curves, OL-OPX and OL-CPX, passing through the S(IV) field (Fig. 11). We suggest that among the S(IV) asteroids are those whose pyroxene is entirely OPX and which therefore correspond to EOC, and those with considerable amounts of CPX correspond to the UOC. In our small population of S(IV) asteroids, based on the presence of a 2.3 μm peak (Fig. 9), we suggest that 6 Hebe, 1620 Geographos, 1999 JV3, and 3288 Seleucus have surfaces resembling UOC, while for 1980 Tezcatlipoca and 2212 Hephaistos this is less clear and these may more closely resemble EOC. Gaffey and Gilbert (1998) have previously linked Hebe with the H chondrites.

No chondritic meteorites, equilibrated or unequilibrated, plot in the S(I), S(II), S(III), S(V), S(VI), or S(VII) fields, and there is no evidence for a relationship between these asteroids and any undifferentiated (nonigneous) meteorites like the ordinary chondrite.

Any discussion of asteroid surfaces would be incomplete without a mention of "space weathering," i.e., exposure to the space environment. The major effect of space weathering on the Moon is the formation of nanophase iron phases that redden the spectrum (McKay et al. 1991). It is usually assumed that the same reddening will occur on asteroids as a result of the exposure of their surfaces to the space environment (Chapman 1996; Binzel et al. 2004b), and experiments involving laser irradiation and ion bombardment have reproduced this process in the laboratory (Sasaki et al. 2002; Brunetto and Strazzulla 2005). There are major differences in the composition and impact environment of the Moon and asteroids (McKay et al. 1991) but space weathering, sometimes related to orbit change and close encounter with the Earth, have been proposed (Binzel et al. 2010; Dell'Oro et al. 2011). Ueda et al. (2002) have reported that simulated space weathering and grain size can affect the position and depth of the olivine and pyroxene mixtures, but the effects are relatively small.

Concepts for Meteorite Parent Bodies

Like the meteorites, asteroids show a wide variety of properties consistent with a wide variety of histories, some meteorites appear primary (i.e., essentially solar in composition altered only by exposure to the space environment) while others appear to be completely differentiated and the product of a wide variety of igneous processes (Gaffey et al. 1993b; Chabot and Haack 2006; McCoy et al. 2006). The heat source for differentiation was most probably radioisotopes, essentially ^{26}Al for bodies several kilometers in size (Lee et al. 1976) and possibly also U, Th, and K for bodies hundreds of kilometers in size (Wood 1967). The amount of heating by ^{26}Al depends not only on size, but time of accretion, increasing the range of possible thermal histories. Some of the possibilities are summarized in Fig. 12.

Early formed or larger objects would differentiate to produce a variety of igneous rocks on their surfaces, metallic objects at their cores, and pallasite (stony iron) meteorites at the core-mantle interface (Fig. 12a). Smaller objects, or objects forming later, might be heated but not melted and differentiated. This scenario is represented by Fig. 12b and is often discussed in connection with the metamorphic history of ordinary chondrites as the "onion skin" model (e.g., McSween and Bennett 1996; Akridge et al. 1998). Objects too small for significant build-up of heat, or objects that formed late, i.e., after the original ^{26}Al had decayed to insignificant levels, would experience little or no internal heating and remain essentially unaltered throughout (Fig. 12c). In the inner asteroid belt, these are the type 3 ordinary chondrites while in the outer belt the equivalent would be the C chondrites and the C and X asteroids (Lunine 2006). Finally, as shown in Fig. 12d, some asteroids experienced fragmentation and reassembly to

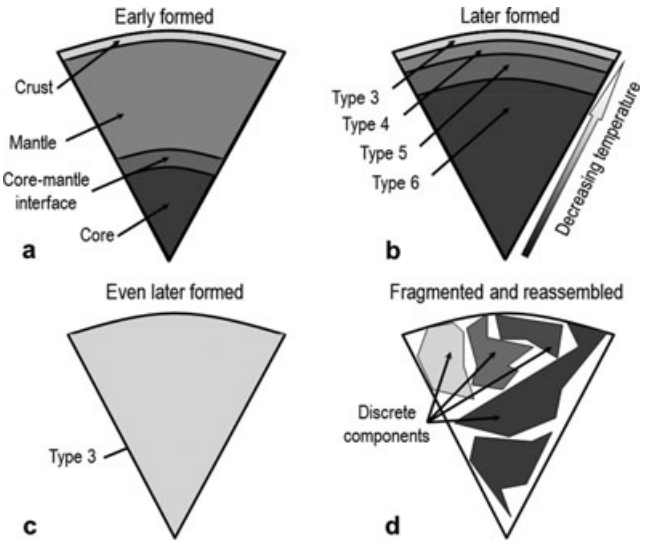

Fig. 12. Schemes for the possible interiors of asteroids. a) Objects that form when ^{26}Al is still present in the solar system and which are large enough will melt and differentiate to form a core, mantle, and crust. Meteorites are known that appear to represent these objects, such as iron meteorites from cores, stony-iron meteorites from the interface, and various differentiated meteorites that represent mantle and crust of their parent asteroids. b) Objects that formed later or were too small to retain enough heat for complete melting will have a heated interior and unheated surface with concentric zoning of metamorphic alteration that increases with depth. The thickness of the layers will depend on composition, amount of ^{26}Al, and—most importantly—the thermal properties of the layers. However, all models predict a volumetrically large amount of type 6 material and relatively smaller amounts of the outer layers, consistent with the observed ordinary chondrite flux to Earth. c) Asteroids forming after decay of ^{26}Al, or too small for significant heating by ^{26}Al, will resemble type 3 material throughout. d) After formation impact could disrupt the object and allow mixing, so the surface would reflect the prior internal nature of the asteroid. We argue that since most asteroids have clinopyroxene on their surfaces, then schemes (a–c) are likely, but since equilibrated (type 4–6) ordinary chondrites are reaching Earth, then scheme (b) must sometimes apply.

produce the rubble piles (Michel et al. 2001). Such seems to be the case with asteroid Itokawa (Fujiwara et al. 2006).

It is interesting to note that asteroids with type 3 surfaces should be common. To produce a body with type 5,6 surfaces requires considerable fragmentation; every asteroid undergoing metamorphism, as opposed to differentiation, will have a type 3 surface. While fragmentation is expected to be common in the asteroid belt, type 5,6 ordinary chondrites seem to be coming from very few fragmented parent objects (see below), so there is no a priori reason to assume type 3 ordinary chondrites are not coming from a large number of parent objects.

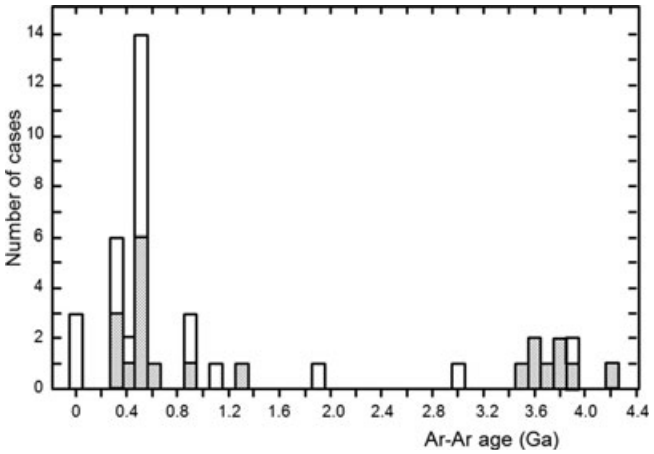

Fig. 13. The distribution of K-Ar age (determined by the Ar-Ar method) for L chondrites shows a large proportion of members with 0.5 Ga ages, suggesting that until this time these meteorites were part of the same parent object. Most of the L chondrites in the 0.5 Ga peak are shock blackened, consistent with a major and violent break-up event. The shading refers to meteorites that have plateaued in their Ar release patterns, and that are probably undisturbed since the event that reset their K-Ar clock. Such data indicate that most or probably all of these meteorites came from the interior of their parent asteroid and would not be observed by astronomical techniques. This diagram is a simplified version of a figure in Bogard (1995).

The Origin and History of EOC and UOC

Probably the best experimental data on asteroid fragmentation history are the ages of meteorites, in particular the K-Ar ages and the cosmic ray exposure ages (Bogard 1995; Eugster et al. 2006). The L chondrites show an often-discussed peak in the K-Ar ages at approximately 500 Ma and the meteorites most clearly showing this age are the shock-blackened ordinary chondrites. Apparently, at this time the L chondrite parent object underwent a major breakup, so that most suffered a complete loss of ^{40}Ar and resetting of their K-Ar ages. Others not as much affected by the heat, maybe those closer to the surface or further from the point of impact, may have suffered less or little heating. Thus, there is a variation in apparent age. These effects can be disentangled to some degree by the Ar-Ar method, which determines the degree of gas loss and identifies those for which a reliable age can be calculated. Figure 13 shows the age distribution for L chondrites determined this way. Apparently, the majority—and probably all—of the L chondrites were produced from the breakup of a single parent object. It is therefore probably that most of the L chondrites are coming from a single source that broke up about 500 Ma ago.

Cosmic ray exposure ages reflect the time at which the bodies became meter sized and penetrable by cosmic radiation (Fig. 14). Prior to that we must assume the

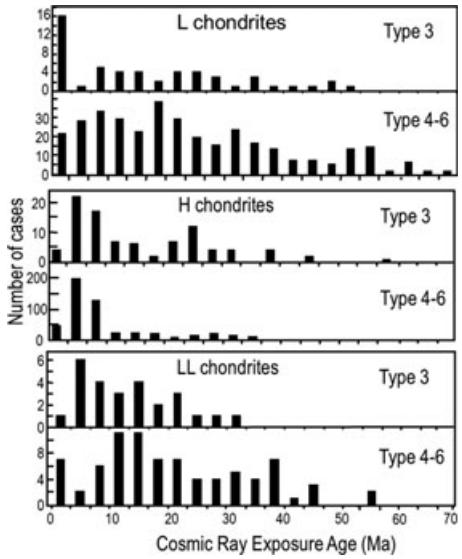

Fig. 14. Cosmic ray exposure ages for ordinary chondrites calculated from ^{21}Ne concentrations obtained from the compilation by Schultz and Franke (2004) assuming a production rate of 0.3×10^{-8} cm^3 STP/(gGa) (Leya et al. 2000). Multiple determinations for a single meteorite have been averaged. For each of the chemical classes, H, L, and LL, the type 3 (unequilibrated) and type 4–6 (equilibrated) ordinary chondrites are shown. The presence of peaks in these histograms suggests meteorite formation by fragmentation of a single parent object. All three chemical classes show differences in the distribution for type 3 compared with type 4–6 suggesting that some fraction came from separate parent objects. Examples are the approximately 25 Ma peak for the H chondrites, the approximately 2 Ma peak for the L chondrites, and the approximately 5 Ma peak for the LL chondrites. Conversely, peaks are sometimes present in the type 4–6 distributions that are absent from the type 3 distributions, such as 52–55 Ma peak for L4–6 chondrites and the approximately 38 Ma peak for LL4–6. The approximately 2 Ma peak for the L3 chondrites may be due to pairing, a large number of meteorite fragments being unrecognized fragments of the same meteorite, but for the H and LL ordinary chondrites there appear to be genuinely different distributions for the type 3 and type 4–6 ordinary chondrites that suggest origins for some fraction of the type 3s on different parent bodies.

bodies were shielded inside larger bodies. It is therefore highly significant that cosmic ray exposure ages for ordinary chondrites are very short, generally less than 100 Ma, again implying that the majority of meteorites came from the interior of bodies recently disrupted. There is also clustering of ages that appear as peaks in the cosmic age distributions. The peak at 8 Ma for the H chondrites, 17 Ma for the LL chondrites, and possibly several peaks at 4, 20, and 50 Ma in the L chondrites have been frequently discussed (Eugster et al. 2006).

If ordinary chondrites are coming from metamorphically zoned asteroids similar to those in Fig. 12b, then one might expect the type 3 chondrites to be coming from any number of asteroids, released by moderately sized impacts. These impacts need not be large enough to disrupt the body, and could be quite gentle. Therefore, they would not be expected to show the same cosmic ray exposure age distribution as the equilibrated ordinary chondrites that required major disruption events, the L chondrites especially.

Figure 14 shows the cosmic ray age histograms for the H3, L3, and LL3 chondrites in comparison with the equilibrated ordinary chondrites. These ages were calculated from the ^{21}Ne data compiled by Schultz and Franke (2004), averaging data for a single meteorite and assuming a production rate or 0.3×10^{-8} cc g^{-1} Ma^{-1} (Leya et al. 2000). For each of the chemical classes, H, L, and LL, there are significant differences between the age distribution of the equilibrated and unequilibrated ordinary chondrites (Table 9). In the case of the H3 chondrites, the peak at 8 Ma that dominates the equilibrated chondrites is still apparent in the unequilibrated ordinary chondrites, but so is a major peak at about 25 Ma which is absent in the equilibrated chondrites (Fig. 14a). For the L3 chondrites there is a major peak at about 2 Ma, which is absent in the equilibrated chondrites (Fig. 14b). For the LL3 chondrites the 17 Ma peak is absent but there is a peak at about 5 Ma that is absent in the equilibrated ordinary chondrites (Fig. 14c).

Since many of these meteorites are finds from highly productive field areas, like the Allan Hills of Antarctica, it is possible that peaks in the relatively small type 3 populations could be the result of unrecognized pairing. Pairing is common among observed falls, and readily recognizable as such, but among the finds of Antarctica or the deserts the abundance of meteorites and their movement by wind and ice flow make it difficult to identify paired fragments and this is a constant issue for statistical studies (Lindstrom and Score 1995). We therefore list in Table 6 the meteorites populating the peaks in the histograms for the type 3 ordinary chondrites that are weak or absent among the peaks in the histograms of type 4–6 ordinary chondrites. For the approximately 25 Ma H3 chondrite peaks, there are several Acfer meteorites and one from the nearby Hammadah al Hamra that could conceivably be paired, but the others are sufficiently dispersed in time and place of fall and properties that this possibility can be eliminated. Even assuming maximum pairing, the difference between the type 3 and the type 4–6 histograms remains. This is not true of the L chondrite histograms, where large number of Allan Hill meteorites of type approximately 3.4 is present that could be paired. Like the H chondrite case, the LL chondrite approximately 5 Ma peak in the histogram type 3 does not appear to be the result of pairing, the meteorites being too separate in

Table 9. Type 3 ordinary chondrites occupying peaks in the cosmic ray exposure age distributions where those peaks are weak or absent in the type 4–6 distributions.

H3 in the approximately 25 Ma peak		L3 in the approximately 2 Ma peak		LL3 in the approximately 5 Ma peak	
Meteorite	Class	Meteorite	Class	Meteorite	Class
Acfer 11	H3.9	ALH 77015	L3.5	Adzhibogdo	LL3-6
Acfer 22	H3.7	ALH 77047	L3.5	Bishunpur	LL3.1
Acfer 204	H3	ALH 77167	L3.4	Dunedin	LL3
Acfer 225	H3	ALH 77214	L3.4	Hammadah al Hamra 93	LL3.9
ALH 78084	H3.9	ALH 77260	L3.5	Manych	LL3.4
Ceniceros	H3.7	ALH 78015	L3.2	Parnallee	LL3.6
Hammadah al Hamra 28	H3.8/4	ALH 78119	L3.5	Semarkona	LL3.0
Prairie Dog Creek	H3.7	ALH 78170	L3.2		
Roosevelt Co. 75	H3.2	ALH 81025	L3.6		
Sharps	H3.4	ALH 81030	L3.4		
Tieschitz	H/L3.6	ALH 81031	L3.4		
		ALH 81032	L3.4		
		ALH 81121	L3.5		
		ALH 88044	L3.4		
		Bovedy	L3		
		Yamato 2133	L3.5		

ALH = Allan Hills.

time and place of fall and petrographic properties. Most of these meteorites are observed falls.

There are also peaks present in the histograms for type 4–6 chondrites that are absent in the histograms for type 3 chondrites, such as the 38 Ma peak in the LL4–6 chondrites and the 52–55 Ma peak in the L4–6 chondrites. Overall, there is reasonable evidence that many of the type 3 ordinary chondrites are not sharing the fragmentation history of their type 4–6 equivalents.

Many factors affect cosmic ray exposure age determination, production rate variations due to shielding and target composition, and errors and uncertainties in the measurement, for example. But a peak is significant and difficult or impossible to create artificially, and must mean a common disruption effect. Similarly, the differences in the distributions of ages for type 3 and type 4–6 in Fig. 14 are greater than indicated, because of uncertainties in classification, both chemical class and petrographic type. These uncertainties tend to smooth out differences. It seems very likely on the basis of Fig. 14 that the type 3 ordinary chondrites are not necessarily coming from the same parent objects that produced the much more common equilibrated ordinary chondrites.

CONCLUSIONS

We report new near-IR spectra for nearly 30 asteroids including many in near-Earth orbits. The asteroids were spread fairly well over the Gaffey et al. (1993) and DeMeo et al. (2009) classes. In an effort to compare the asteroids with ordinary chondrites, in particular the type 3 or unequilibrated ordinary chondrites (UOC), we compared the spectra of the type 4–6 or equilibrated ordinary chondrites (EOC) with the spectra for the UOC. We observed, first with the naked eye and then with spectrum analysis using the MGM software of Sunshine and Pieters (1993), that UOC and EOC have different near-IR spectra, the former having a peak at 2.3 μm which is not present in the latter. We suggest that this difference is due to the presence of low-Ca clinopyroxene in the UOC but not EOC. This is consistent with the mineralogy and petrology of the meteorites and near-IR reflectance spectra of terrestrial low-Ca clinopyroxenes.

We plotted the EOC and UOC data on the BAR plot and all plotted in or near the S(IV) field of Gaffey et al. (1993a). These data are consistent with some fraction of the S(IV) asteroids having UOC material on their surfaces. We propose that asteroid surface and interior models suggests that UOC material should be present on the surfaces of many asteroids and EOC material present at depth. Ar-Ar ages and cosmic ray exposure ages for equilibrated ordinary chondrites suggest that they came from a few parent objects and that those objects broke up fairly recently, within a few 100 Ma of the present. The cosmic ray exposure data suggest that the UOC and EOC did not share a common fragmentation history. We argue that while EOC come from a relatively small number of objects that broke up fairly recently, UOC come from these objects and from a wide variety of other unrelated objects.

Acknowledgments—Without implying endorsement of our views, we gratefully acknowledge the many colleagues who have commented on our work over the last few years or otherwise helped as we evolved our thoughts and ideas: Paul Abell, Rick Binzel, Vincent Chevrier, Mike Gaffey, Paul Hardersen, Tim McCoy, Andy Rivkin, Ludolf Schultz, and Jessica Sunshine. We are also grateful to NASA for access to the IRTF and for funding, to Bobby Bus for hospitality and help in obtaining the data, Dan Britt for advice using the facility, Takahiro Hiroi for obtaining spectra for terrestrial clinopyroxenes, and Tom Burbine, Beth Clark Joseph, and Hazel Sears for very helpful reviews, and Hazel Sears for proofing the paper.

Editorial Handling—Dr. A. J. Timothy Jull

REFERENCES

Akridge G., Benoit P. H., and Sears D. W. G. 1998. Regolith and megaregolith formation of H-chondrites: Thermal constraints on the parent body. *Icarus* 132:5–195.

Belton M. J. S., Veverka J., Thomas P., Helfenstein P., Simonelli D., Chapman C., Davies M. E., Greeley R., Greenberg R., and Head J. 1992. Galileo encounter with 951 Gaspra—First pictures of an asteroid. *Science* 257:1647–1652.

Belton M. J. S., Chapman C. R., Veverka J., Klaasen K. P., Harch A., Greeley R., Greenberg R., Head J. W., III, McEwen A., Morrison D., Thomas P. C., Davies M. E., Carr M. H., Neukum G., Fanale F. P., Davis D. R., Anger C., Gierasch P. J., Ingersoll A. P., and Pilcher C. B. 1994. First images of asteroid 243 Ida. *Science* 265:1543–1547.

Belton M. J. S., Morgan T. H., Samarasinha N. H., and Yeomans D. K., eds. 2004. *Mitigation of hazardous comets and asteroids*. Cambridge, UK: Cambridge University Press.

Binzel R. P., Xu S., Bus S. J., Skrutskie M. F., Meyer M. R., Knezek P., and Barker E. S. 1993. Discovery of a main-belt asteroid resembling ordinary chondrite meteorites. *Science* 262:1541–1543.

Binzel R. P., Harris A. W., Bus S. J., and Burbine T. H. 2001. Spectral properties of near-Earth objects: Palomar and IRTF results for 48 objects including spacecraft targets 9969. Braille and 10302. 1989 ML. *Icarus* 151:139–149.

Binzel R. P., Perozzi E., Rivkin A. S., Rossi A., Harris A. W., Bus S. J., Valsecchi G. B., and Slivan S. M. 2004a. Dynamical and compositional assessment of near-Earth object mission targets. *Meteoritics & Planetary Science* 39:351–366.

Binzel R. P., Rivkin A. S., Stuart J. S., Harris A. W., Bus S. J., and Burbine T. H. 2004b. Observed spectral properties of near-Earth objects: Results for population distribution, source regions, and space weathering processes. *Icarus* 170:259–294.

Binzel R. P., Morbidelli A., Merouane S., DeMeo F. E., Birlan M., Vernazza P., Thomas C. A., Rivkin A. S., Bus S. J., and Tokunaga A. T. 2010. Earth encounters as the origin of fresh surfaces on near-Earth asteroids. *Nature* 463:331–334.

Bogard D. D. 1995. Impact ages of meteorites: A synthesis. *Meteoritics* 30:244–268.

Bottke W. F., Jr., Cellino A., Paolicchi P., and Binzel R. P. eds. 2002. *Asteroids III*. Tucson, Arizona: The University of Arizona Press.

Brunetto R. and Strazzulla G. 2005. Elastic collisions in ion irradiation experiments: A mechanism for space weathering of silicates. *Icarus* 179:265–273.

Buchanan P. C. and Reid A. M. 1996. Petrology of the polymict eucrite Petersburg. *Geochimica et Cosmochimica Acta* 60:135–146.

Burbine T. H., McCoy T. J., Meibom A., Gladman B., and Keil K. 2002. Meteoritic parent bodies: Their number and identification. In *Asteroids III*, edited by Bottke W. F., Jr., Cellino A., Paolicchi P. and Binzel R. P. Tucson, Arizona: The University of Arizona Press. pp. 653–667.

Bus S. J. and Binzel R. P. 2002. Phase II of the small main-belt asteroid spectroscopic survey: The observations. *Icarus* 158:106–145.

Bus S. J., Vilas F., and Barucci M. A. 2002. Visible-wavelength spectroscopy of asteroids. In *Asteroids III*, edited by Bottke W. F., Jr., Cellino A., Paolicchi P. and Binzel R. P. Tucson, Arizona: The University of Arizona Press. pp. 169–182.

Chabot N. L. and Haack H. 2006. Evolution of asteroidal cores. In *Meteorites and the early solar system II*, edited by Lauretta D. S. and McSween H. Y., Jr. Tucson, Arizona: The University of Arizona Press. pp. 747–771.

Chapman C. R. 1996. S-type asteroids, ordinary chondrites, and space weathering: The evidence from Galileo's fly-bys of Gaspra and Ida. *Meteoritics* 31:699–725.

Clénet H., Pinet P., Daydou Y., Heuripeau F., Rosemberg C., Baratoux D., and Chevrel S. 2011. A new systematic approach using the modified Gaussian model: Insight for the characterization of chemical composition of olivines, pyroxenes and olivine-pyroxene mixtures. *Icarus* 213:404–422.

Cochran A. L., Vilas F., Jarvis K. S., and Kelley M. S. 2004. Investigating the Vesta-vestoid-HED connection. *Icarus* 167:360–368.

Deer W. A., Howie R. A., and Zussman J. 1996. *An introduction to the rock-forming minerals, 2nd ed*. Harlow, UK: Prentice Hall.

Dell'Oro A., Marchi S., and Paolicchi P. 2011. Collisional evolution of near-Earth asteroids and refreshing of the space-weathering effects. *Monthly Notices of the Royal Astronomical Society: Letters* 416:L26–L30.

DeMeo F. E., Binzel R. P., Slivan S. M., and Bus S. J. 2009. An extension of the Bus asteroid taxonomy into the near-infrared. *Icarus* 202:160–180.

Dodd R. T., Koffman D. M., and van Schmus W. R. 1967. A survey of the unequilibrated ordinary chondrites. *Geochimica et Cosmochimica Acta* 31:921–934.

Drake M. J. 2001. The eucrite/Vesta story. *Meteoritics & Planetary Science* 36:501–513.

Duke M. B. and Silver L. T. 1967. Petrology of eucrites, howardites and mesosiderites. *Geochimica et Cosmochimica Acta* 31:1637–1642.

Eugster O., Herzog G. F., Marti K., and Caffee M. W. 2006. Irradiation records, cosmic-ray exposure ages, and transfer times of meteorites. In *Meteorites and the early solar system II*, edited by Lauretta D. S. and McSween H. Y., Jr. Tucson, Arizona: The University of Arizona Press. pp. 829–851.

Farquhar R., Kawaguchi J., Russell C., Schwehm G., Veverka J., and Yeomans D. 2002. Spacecraft exploration of asteroids: The 2001 perspective. *Asteroids III*, edited by Bottke W. F., Jr., Cellino A., Paolicchi P., and Binzel R. P. Tucson, Arizona: The University of Arizona Press. pp. 367–376.

Feierberg M. A. and Drake M. J. 1980. The meteorite-asteroid connection—The infrared spectra of eucrites, shergottites, and Vesta. *Science* 209:805–807.

Fujiwara A., Kawaguchi J., Yeomans D. K., Abe M., Mukai T., Okada T., Saito J., Yano H., Yoshikawa M., Scheeres D. J., Barnouin-Jha O., Cheng A. F., Demura H., Gaskell R. W., Hirata N., Ikeda H., Kominato T., Miyamoto H., Nakamura A. M., Nakamura R., Sasaki S., and Uesugi K. 2006. The rubble-pile asteroid Itokawa as observed by Hayabusa. *Science* 312:1330–1334.

Gaffey M. J. 1976. Spectral reflectance characteristics of the meteorite classes. *Journal of Geophysical Research* 81:905–920.

Gaffey M. J. 2007. Where are all the partially melted meteorites? *Meteoritics & Planetary Science Supplement* 42:A5296.

Gaffey M. J. and Gilbert S. L. 1998. Asteroid 6 Hebe: The probable parent body of the H-type ordinary chondrites and the IIE iron meteorites. *Meteoritics & Planetary Science* 33:281–295.

Gaffey M. J., Bell J. F., Brown R. H., Burbine T. H., Piatek J. L., Reed K. L., and Chaky D. A. 1993a. Mineralogical variations within the S-type asteroids class. *Icarus* 106:573–602.

Gaffey M. J., Burbine T. H., and Binzel R. P. 1993b. Asteroid spectroscopy: Progress and perspective. *Meteoritics* 28:161–187.

Gaffey M. J., Cloutis E. A., Kelley M. S., and Reed K. L. 2002. Mineralogy of asteroids. In *Asteroids III*, edited by Bottke W. F., Jr., Cellino A., Paolicchi P. and Binzel R. P. Tucson, Arizona: The University of Arizona Press. pp. 183–204.

Gastineau-Lyons H. K., McSween H. Y., Jr., and Gaffey M. J. 2002. A critical evaluation of oxidation versus reduction during metamorphism of L and LL group chondrites, and implications for asteroid spectroscopy. *Meteoritics & Planetary Science* 37:75–89.

Gietzen K. M. and Lacy C. H. S. 2007. Visible and near infrared spectra of main belt and near Earth asteroids (abstract #1104). Proceedings, 38th Lunar and Planetary Science Conference. CD-ROM.

Gietzen K. M., Lacy C. H., and Rivkin A. S. 2006. Visible and near infrared spectra of five near Earth asteroids. American Astronomical Society Meeting 208, #11.02. *Bulletin of the American Astronomical Society* 38:90.

Gietzen K. M., Lacy C. H., and Sears D. W. 2007. Abundant clinopyroxene on the S asteroids and implications for meteorites and asteroid history and the asteroid-meteorite relationship. American Astronomical Society, DPS meeting #39, #33.11. *Bulletin of the American Astronomical Society* 39:478.

Gietzen K. M., Lacy C. H. S., Ostrowski D. R., and Sears D. W. G. 2008. Analysis of reflectance spectra of ordinary chondrites: Implications for asteroids (abstract #1125). Proceedings, 39th Lunar and Planetary Science Conference. CD-ROM.

Gietzen K. M., Lacy C. H. S., Ostrowski D. R., and Sears D. W. G. 2009. Low-calcium and calcium-free clinopyroxene spectra and the implications for UOC material on asteroids (abstract #1348). 40th Lunar and Planetary Science Conference. CD-ROM.

Hilton J. L. 2002. Asteroid masses and densities. In *Asteroids III*, edited by Bottke W. F., Jr., Cellino A., Paolicchi P. and Binzel R. P. Tucson, Arizona: The University of Arizona Press. pp. 103–112.

Kanner L. C., Mustard J. F., and Gendrin A. 2007. Assessing the limits of the modified Gaussian model for remote spectroscopic studies of pyroxenes on Mars. *Icarus* 187:442–456.

Klima R. L., Pieters C. M., and Dyar M. D. 2007. Spectroscopy of synthetic Mg-Fe pyroxenes I: Spin-allowed and spin-forbidden crystal field bands in the visible and near-infrared. *Meteoritics & Planetary Science* 42:235–253.

Klima R. L., Dyar M. D., and Pieters Carlé M. 2011. Near-infrared spectra of clinopyroxenes: Effects of calcium content and crystal structure. *Meteoritics & Planetary Science* 46:379–395.

Lee T., Papanastassiou D. A., and Wasserburg G. J. 1976. Demonstration of Mg-26 excess in Allende and evidence for Al-26. *Geophysical Research Letters* 3:41–44.

Leya I., Graf T., Nishiizumi K., Günther D., and Wieler R. 2000. Cosmogenic ^{21}Ne production rates in H-chondrites based on ^{36}Cl-^{36}Ar ages (abstract #1562). 31st Lunar and Planetary Science Conference. CD-ROM.

Lindstrom M. M. and Score R. 1995. Populations, pairing, and rare meteorites in the U. S. antarctic meteorite collection. In *Workshop on meteorites from cold and hot deserts, proceedings of the workshop held 20–22 July, 1994 at Nördlingen, Germany*, edited by Schultz L., Annexstad J. O., and Zolensky M. E.. LPI Technical Report 95-02. Houston, Texas: Lunar and Planetary Institute. p. 43.

Lunine J. I. 2006. Origin of water ice in the solar system. In *Meteorites and the early solar system II*, edited by Lauretta D. S. and McSween H. Y., Jr. Tucson, Arizona: The University of Arizona Press. pp. 309–319.

Mayne R. G., McSween H. Y., Jr., McCoy T. J., and Gale A. 2009. Petrology of the unbrecciated eucrites. *Geochimica et Cosmochimica Acta* 73:794–819.

McCord T. B., Adams J. B., and Johnson T. V. 1970. Asteroid Vesta: Spectral reflectivity and compositional implications. *Science* 178:1445–1447.

McCoy T. J., Mittlefehldt D. W., and Wilson L. 2006. Asteroid differentiation. In *Meteorites and the early solar system II*, edited by Lauretta D. S. and McSween H. Y., Jr. Tucson, Arizona: The University of Arizona Press. pp. 733–745.

McKay D. S., Heiken G., Basu A., Blanford G., Simon S., Reedy R., French B. M., and Papike J. 1991. The lunar regolith. In *Lunar sourcebook: A user's guide to the moon*, edited by Heiken G. H., Vaniman D. T., and French B. M. Cambridge: Cambridge University Press. pp. 285–356.

McSween H. Y., Jr. and Bennett M. E. 1996. Revised model calculations for the thermal histories of ordinary chondrite parent bodies. *Meteoritics & Planetary Science* 31:783–792.

Michel P., Benz W., Tanga P., and Richardson D. C. 2001. Collisions and gravitational reaccumulation: Forming asteroid families and satellites. *Science* 294:1696–1700.

Rayner J. T., Toomey D. W., Onaka P. M., Denault A. J., Stahlberger W. E., Vacca W. D., Cushing M. C., and Wang S. 2003. SpeX: A medium-resolution 0.8–5.5 micron spectrograph and imager for the NASA infrared telescope facility. *Publications of the Astronomical Society of the Pacific* 115:362.

Robinson M. S., Thomas P. C., Ververka J., Murchie S. L., and Wilcox B. B. 2002. The geology of Eros. *Meteoritics & Planetary Science* 37:1651–1684.

Sasaki S., Hiroi T., Nakamura K., Hamabe Y., Kurahashi E., and Yamada M. 2002. Simulation of space weathering by nanosecond pulse laser heating: Dependence on mineral composition, weathering trend of asteroids and discovery of nanophase iron particles. *Advances in Space Research* 29:783–788.

Schultz L. and Franke L. 2004. Helium, neon, and argon in meteorites: A data collection. *Meteoritics & Planetary Science* 39:1889–1890.

Sears D. W. G., Huang S., and Benoit P. H. 1996. Open-system behaviour during chondrule formation. In *Chondrules and the protoplanetary disk*, edited by Hewins R. H., Jones R. H., and Scott E. R. D. Cambridge: Cambridge University Press. pp. 221–231.

Sears D. W. G., Gietzen K., Ostrowski D., Lacy C., and Chevrier V. 2008. Primitive materials on asteroids. 71st Annual Meeting of the Meteoritical. *Meteoritics & Planetary Science* 43:1–1. (Abstract #5237)

Sullivan R., Grelley R., Pappalardo R., Asphaug E., Moore J. M., Morrison D., Belton M. J. S., Carr M., Chapman C. R., Geissler P., Greenberg R., Granahan J., Head J. R., Kirk R., McEwen A., Lee P., Thomas P. C., and Veverka J. 1996. Geology of 243 Ida. *Icarus* 142:89–96.

Sunshine J. M. and Pieters C. M. 1993. Estimating modal abundances from the spectra of natural and laboratory pyroxene mixtures using the modified Gaussian model. *Journal of Geophysical Research* 98:9075–9087.

Sunshine J. M., Pieters C. M., and Pratt S. F. 1990. Deconvolution of mineral absorption bands: An improved approach. *Journal of Geophysical Research* 95:6955–6966.

Sunshine J. M., Bus S. J., McCoy T. J., Burbine T. H., Corrigan C. M., and Binzel R. P. 2004. High-calcium pyroxene as an indicator of igneous differentiation in asteroids and meteorites. *Meteoritics & Planetary Science* 39:1343–1357.

Tholen D. J. 1989. *Asteroid taxonomic classifications in Asteroids II*. Tucson, Arizona: The University of Arizona Press. pp. 1139–1150.

Thomas P. C., Veverka J., Bell J. F., Clark B. E., Carcich B., Joseph J., Robinson M., McFadden L. A., Malin M. C., Chapman C. R., Merline W., and Murchie S. 1999. Mathilde, size, shape and geology. *Icarus* 140:17–27.

Thomas P. C., Joseph J., Robinson M., Murchie S., Veverka J., Clark B. E., and Chapman C. R. 2002. Shape, slopes, and slope processes on Eros. *Icarus* 155:18–37.

Ueda Y., Hiroi T., Pieters C. M., and Miyamoto M. 2002. Changes of Band I center and Band II/Band I area ratio in reflectance spectra of olivine-pyroxene mixtures due to the space weathering and grain size effects (abstract #2023). 33rd Annual Lunar and Planetary Science Conference. CD-ROM.

Van Schmus W. R. and Wood J. A. 1967. A chemical-petrologic classification for the chondritic meteorites. *Geochimica et Cosmochimica Acta* 31:747–765.

Wood J. A. 1967a. Chondrites: Their metallic minerals, thermal histories, and parent planets. *Icarus* 6:1–49.

Wood J. A. 1967b. The early thermal history of planets: Evidence from meteorites. In *Mantles of the Earth and terrestrial planets*, edited by Runcorn S. K. London: Published by Interscience Publishers, a division of John Wiley & Sons. 3 p.

Xu S., Binzel R. P., Burbine T. H., and Bus S. J. 1995. Small main-belt asteroid spectroscopic survey: Initial results. *Icarus* 115:1–35.